Classical backpropagation for probing the backward rescattering time of a tunnel-ionized electron in an intense laser field

Yang Hwan Kim,[1,2] Igor A. Ivanov,[1] and Kyung Taec Kim[1,2,*]

[1]*Center for Relativistic Laser Science, Institute for Basic Science, Gwangju 61005, Korea*

[2]*Department of Physics and Photon Science, Gwangju Institute of Science and Technology, Gwangju 61005, Korea*

(Received 26 March 2021; accepted 13 July 2021; published 26 July 2021)

We present a method to estimate the backward rescattering time of a tunnel-ionized electron in an intense laser pulse. The idea of the classical backpropagation method is applied to determine the backward rescattering time and its dependence on various parameters such as the ionization potential of the parent ion, its spatial profile and the peak intensity and wavelength of the driving laser field. The accurate estimation of the rescattering time would provide critical information in analyzing ultrafast rescattering dynamics in applications such as high-order harmonic generation, above-threshold ionization, and laser-induced electron diffraction experiments. We find that the backward rescattering time is significantly affected by the peak intensity of the laser pulse. The rescattering time changes by a few hundred attoseconds when the peak intensity varies from 1×10^{14} to 5×10^{14} W/cm^2.

DOI: 10.1103/PhysRevA.104.013116

I. INTRODUCTION

Understanding strong-field phenomena requires an accurate description of the ultrafast electron dynamics in an intense laser field. When an atom interacts with an intense laser field, a valence electron can tunnel out every half optical cycle [1–3]. Subsequently, the electron can be driven back to the parent ion when the sign of the laser field is reversed in the next half optical cycle. The returning electron can rescatter or recombine with the parent ion. The recombination of the electron results in EUV or soft X-ray emissions generated through high-order harmonic generation (HHG) [4–11] and frustrated tunneling ionization [12–14]. Electron rescattering is responsible for the formation of the high energy electrons in the above-threshold ionization (ATI). The rescattered electron provides thus critical information on the parent ion in the ATI process [15–20], and related phenomena such as laser-induced electron diffraction (LIED) [21–25] or other phenomena accompanying strong-field ionization [26–28]. Therefore, an accurate description of rescattering or recombination processes is of great importance.

An important parameter characterizing rescattering is the rescatternig time. It determines the phase of extreme ultraviolet emission in HHG known as attochirp [29,30], the energy of ATI electrons in an ATI photoelectron spectrum [17–19], and the phase accumulation of the diffracted electrons in LIED experiments.

A full *ab initio* description of the ultrafast electron dynamics can be provided by the time-dependent Schrodinger equation (TDSE). A solution of the TDSE provides exact information on the evolution of the electronic wave function in an intense laser field for simple atoms such as H and He and reasonably good approximations even for complicated atoms [31,32]. However, it is challenging to extract quantitative information from the evolution of the wave function for the description of the ultrafast electron dynamics. One approach to analyze the electron's trajectories using the solution of the TDSE is to use Bohmian mechanics [33–35]. However, it only provides the trajectories corresponding to the total wave function, not the trajectories corresponding to ionized wave packets produced at each half optical cycle of the laser pulse. Therefore, it is difficult to obtain a clear intitutive interpretation of ionization dynamics using the solution obtained by solving the TDSE.

To introduce the notion of rescattering time we must reintroduce the concept of an electron trajectory in some form. This can be done, for instance, basing on the picture of ionization provided by the strong-field approximation (SFA) model or trajectory-based semiclassical models developed for the description of the strong field dynamics of a tunneling ionization [36–38]. While a clear physical picture of the trajectories can be obtained using these approaches, the results obtained by the SFA model are highly dependent on the initial conditions assumed at the birth time. Also, in the framework of the SFA model and the quantum orbits approach it is difficult to consider the influence of the atomic potential.

Recently, the classical backpropagation method has been proposed [39–43], which provides a consistent theoretical framework allowing to reintroduce trajectories in quantum mechanics. The classical backpropagation method combines advantages provided by the two approaches, the TDSE and the semiclassical approach. First, the evolution of the wave function is obtained by solving the TDSE which provides accurate information on the ultrafast electron dynamics, including tunneling and rescattering in an intense laser field. Then, the electron trajectory is backpropagated by solving Newton's equation of motion, in which the Coulomb potential is taken

*kyungtaec@gist.ac.kr

 ©2021 American Physical Society

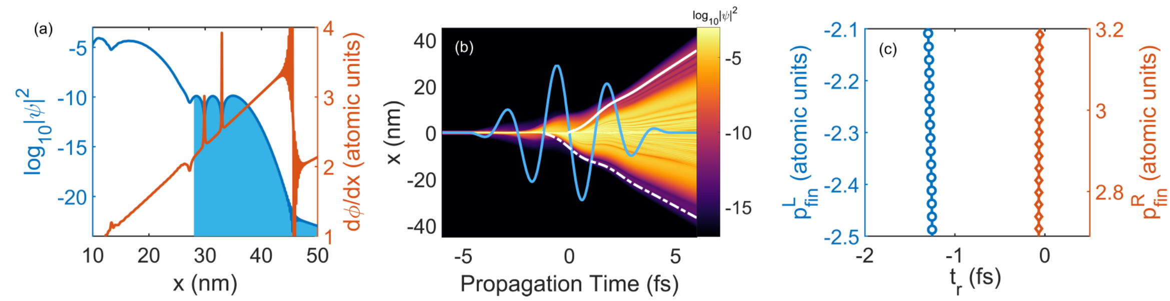

FIG. 1. Concept of the classical backpropagation for probing backward rescattering time. (a) Electron probability distribution (blue line) calculated by solving the TDSE and spatial derivative of phase (red line) in Ar. The blue area is the region where the classical backpropagation method is applied. (b) Evolution of an electron wave function colored in the logarithmic scale with an electric field (blue solid line) and electron trajectories (white solid and dashed lines) obtained using the classical backpropagation. The wave function shown in (a) is the part of the wave function shown in (b) at the end of the propagation time. (c) Backward rescattering times t_r obtained for different final momenta using the classical backpropagation for the right direction (red line with diamonds, $x > 0$) and the left direction (blue line with circles, $x < 0$). Note that the range of the y axis for the left and the right directions are different. A cos-squared envelope for the laser pulse as $E(t) \propto \cos^2(\pi t/4T_1)\cos(2\pi t/T_1 + \phi_{CEP})$. Here, the center wavelength is 800 nm, T_1 is 2.6 fs, and ϕ_{CEP} is 0.5π. The peak intensity is 2.0×10^{14} W/cm^2.

into account, with the initial (or rather final) conditions provided by the solution of the TDSE. The backpropagation stops when the tunneling criterion is met [39]. In this way, the tunneling time has been determined in an unambiguous way in an attosecond angular streaking configuration [39–41].

In the present work, we use the idea of the classical backpropagation method to estimate a backward rescattering time (BRT) for the process of tunneling ionization in an intense laser field. We study the dependence of the BRTs on various factors, such as the peak intensity and the center wavelength of the driving laser field, the ionization potential of the target ion and the spatial profile of the ionic potential. We find that the peak intensity is the most essential parameter that determines the BRT. An accurate estimation of the BRT will provide useful information in applications such as LIED, attosecond holography, and HHG.

This paper is organized as follows. A brief description of the semiclassical picture of the backward rescattering dynamics is given in Sec. II A. The concept of the classical backpropagation method and its application to BRT is described in Sec. II B. The BRTs obtained for different laser parameters and ionic potential shapes are analyzed in Sec. III. The carrier-envelope phase (CEP) dependence of the BRT is presented in Sec. III A. The BRTs obtained for different ionization potentials and peak intensities are discussed in Sec. III B. The BRT dependences on the ionic potentials width and laser center wavelengths presented in Sec. III C. Finally, we discuss the results and present conclusions in Sec. IV.

II. CLASSICAL BACKPROPAGATION AND BACKWARD RESCATTERING TIME

A. Semiclassical description of backward rescattering dynamics

An electron bound to an atom interacting with an intense laser field can tunnel out through the potential barrier formed by the superposition of the Coulomb field of the parent ion and the laser field [3,44]. Using the simple classical picture provided by the well-known simple man model (SMM) [2,3] the subsequent electron's behavior can be described as follows. Depending on the ionization time the electron may follow different paths. Electron can be driven away (the so-called direct electrons) from the parent ion if the ionization time belongs to the interval when electric field of the pulse increases [12–14]. Or, if ionization time belongs to the interval when the field decreases, the electron can be driven back (the so-called rescattered electrons) to the parent ion as the sign of the laser field is reversed. When the electron returns to the parent ion, it can be rescattered in the forward or backward directions.

Both the direct electrons and the forward rescattered electrons can gain the kinetic energy up to $2U_p$, where U_p is the ponderomotive energy. On the other hand, the backward rescattered electron can gain the kinetic energy up to $10U_p$. Therefore, such electrons are clearly distinguished in the ATI energy spectrum, as shown in Fig. 1(a). Note that both the $2U_p$ and $10U_p$ are the upper limits of the kinetic energy in the classical description, the electron can gain kinetic energy exceeding these limits with low probability in the quantum mechanical description.

From now on we concentrate on the trajectories of the rescattered electrons. The rescattering time satisfies the following condition [45]:

$$\int_{t_i}^{t_r} A(t)dt = (t_r - t_i)A(t_i), \tag{1}$$

where A is vector potential of the laser field. t_i and t_r are ionization time and rescattering time, respectively. Here, any influence of the ionic potential on the electron is neglected. Depending on the laser pulse duration, the backward rescattering events leading to the same final electron momentum may occur one or several times during the pulse duration. Therefore, either a continuum or an interference pattern can be observed in a photoelectron spectrum measured along the polarization direction of the laser field around the cutoff energy $10U_p$ depending on the CEP of the few-cycle laser pulse [17,19], because the backward rescattering event occurs once in every half-cycle of the laser field, and the direction of the rescattering is reversed for the consecutive half cycles. If the backward rescattering in a given direction occurs only once, a continuum spectrum is observed near the cutoff energy, and a specific half cycle of the laser field in which the backward rescattering occurs can be specified. In the present work, we set the pulse duration to be shorter than two cycles and analyze the continuum spectrum observed at the cutoff.

B. Classical backpropagation

We use the idea of the classical backpropagation [39–41] to estimate the timing when the backward rescattering occurs. This approach has been used in Refs. [39–41] to analyze the tunneling ionization time. The method combines the advantages of both quantum mechanical and classical approaches. The quantum mechanical processes such as ionization and rescattering are taken into account by accurately propagating the TDSE forward in time on the interval of pulse duration. Then, the classical trajectories are obtained by propagating Newton's equation of motion backward in time.

We study electron dynamics in one dimension. Since we are interested in the backward rescattered electron in the linearly polarized laser field, the one-dimensional (1D) approach is justified. We used a sufficiently large spatial and temporal grids to avoid reflection at the absorbing boundaries of the spatial grid. For example, we solved the 1D TDSE with the total number of time steps $N_t = 32769$ with the time step size of 0.015 atomic unit, resulting in the total interval (−6 fs, 6 fs) of time propagation. We used the spatial grid of $N_x = 16385$ steps with the grid size of 0.23 atomic units, resulting in the total spatial domain of ±200 nm for the center wavelength of the laser field of 800 nm. The grid size was adjusted when the wavelength was changed. The calculations results are shown in Fig. 1.

After propagating the wave function till the end of the laser pulse, we use the recipe of the backpropagation technique [39] to set initial conditions for the backpropagation method. We use the first spatial derivative of the phase of the wave function to determine the local-momentum of the electron, as shown in Fig. 1(a) [46]. The local-momenta and positions in the shaded region in Fig. 1(a) were taken as the initial conditions for propagating Newton's equation of motion in the backward direction in time, as shown in Figs. 1(a) and 1(b). Newton's equation of motion were solved with a negative time step, and the calculation was stopped when the trajectory reached the core of the potential ($x = 0$). The moment of time when the propagation stops is taken as the time of the backward rescattering, Figs. 1(b) and 1(c). In this way, the BRTs for the final local velocities in the region of interest can be obtained. Note that the rescattering time is distributed narrowly around the time when electric field of the pulse passes through zero (the zero-crossing time) for a wide range of final local momenta, as shown in Fig. 1(c).

In contrast to the case when circularly polarized pulses are used [39], the interference of the electron wave packet following short and long rescattering paths makes dips (at 30 and 33 nm) in the blue shaded region in Fig. 1(a). It is difficult to determine the phase gradient near the dips. However, the two quantum trajectories merge at the cutoff near $10U_p$ and the phase gradient above the cutoff energy can be uniquely determined. Therefore, we can apply the classical backpropagation method using a linearly polarized pulses.

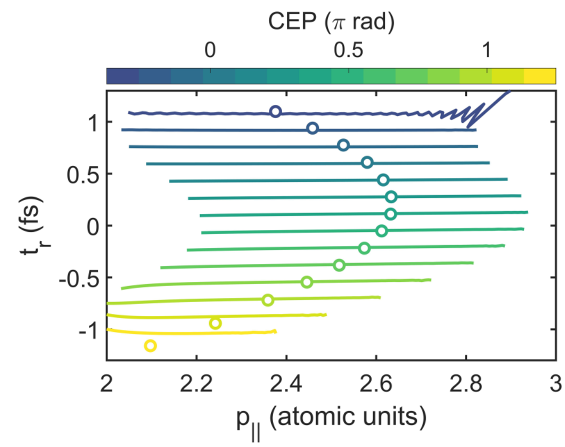

FIG. 2. BRTs of an electron gaining high energy in Ar going out to the right ($x > 0$) for 14 different CEPs. Solid lines are BRTs obtained by the classical backpropagation and circles are BRTs obtained by the simple man model. Gaussian enveloped, 3 fs full width at half maximum electric field with peak intensity of $1 \times 10^{14}\ \mathrm{W/cm^2}$, and center wavelength of 800 nm was used to obtain the results.

III. RESULTS

A. Carrier-envelope phase dependence

Since the BRTs of the electron gaining high kinetic energy are distributed around the zero-crossing time of the driving electric field, the BRT shifts as CEP varies. The BRTs obtained for the different CEPs of the laser field in Ar for the final electron momentum in the right direction ($x > 0$) are shown in Fig. 2. The small oscillations observed near t ∼ 1 fs are due to small numerical errors. One can see the BRTs are distributed narrowly near the zero-crossing time of the electric field. The BRTs are shifted as the CEP varies as expected.

As shown in Fig. 2 the results obtained by the classical backpropagation method are consistent with the results predicted by the SMM (circles in Fig. 2). However, some differences can also be found between the predictions of two methods. For the high CEP values, the BRTs calculated by the backpropagation method are earlier than those obtained by using the SMM. The difference is clearly observed when $t_r \sim -1$ fs. For low CEP values, the BRTs obtained by the classical backpropagation method are slightly later than those obtained by using the SMM. These differences can be caused due to the different intensities between the ionization time and the rescattering time for different CEPs. As the CEP varies, the electron can be ionized at the beginning of the laser pulse where the intensity is low, or at the center of the pulse where the intensity is high. In addition, it should be noted that the atomic potential is completely ignored in the SMM. We need, therefore, to analyze the effect of the ionic potential and the peak intensity of the driving laser pulse on the BRTs.

B. Ionization potential and peak intensity dependence

In order to estimate the effect of the ionic potential on the BRTs, we compared classical backpropagation results obtained for five different soft-core potentials, as shown in Fig. 3(a). The ground state energies of each soft-core poten-

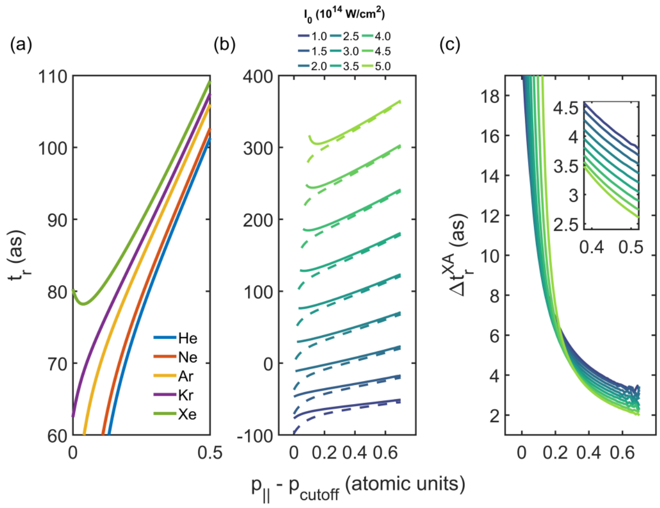

FIG. 3. Potential profile and intensity dependence of BRTs obtained by the classical backpropagation. (a) Potential profile dependence of BRT of the electron at the cutoff. Electric field with the peak intensity of 2.5×10^{14} W/cm^2, the center wavelength of 730 nm, and the CEP of 0.5π was used to obtain the result. (b) Intensity dependence of BRTs of the electron for nine different intensities. The BRTs obtained for Ar (dashed lines) and Xe (solid lines) are compared. (c) Difference between the BRTs of the electron in the high energy plateau for Ar and Xe potential, where $\Delta t_r = t_r^{\mathrm{Xe}} - t_r^{\mathrm{Ar}}$. For all intensities from 1.0×10^{14} to 5.0×10^{14} W/cm^2, the BRTs of the electron in the high energy plateau for Ar is earlier in time than that for Xe. Inset: magnified plot $p_{||} - p_{\mathrm{cutoff}}$ between 0.38 and 0.52 atomic units.

tial correspond to the ionization potential of He, Ne, Ar, Kr, and Xe. As one can see, for each local-momentum relative to the cutoff momentum $p_{\mathrm{cutoff}} = \sqrt{20U_p}$, the BRTs increase monotonously with the ionization potential. In other words, the rescattering time is the earliest in He and the latest in Xe.

The other feature observed in the presence of the potential is that the BRT is dependent on the peak intensity of the laser field. In the simple man model, this dependency is absent because the rescattering condition (1) contains the vector potential of the laser field linearly. However, if the atomic potential is included, the rescattering condition of the electron is no longer a simple linear equation. In addition, the initial positions and initial momenta of the electron at the ionization time also depend on the peak intensity when the potential is included. Therefore, the BRTs can vary depending on both the peak intensity and the ionization potential.

For more detailed analysis, we compared the BRTs calculated for different intensities in Ar and Xe, as shown in Fig. 3(b). The BRTs are delayed when the peak intensity of the laser field increases for both potentials. The BRTs in Ar are earlier than those in Xe for the peak intensities between 1×10^{14} W/cm^2 and 5×10^{14} W/cm^2. The BRTs at the peak intensities greater than 2.0×10^{14} W/cm^2 are even later than the zero-crossing time of the electric field for both Xe and Ar. The BRTs depend on the peak intensity of the laser field quite dramatically, and they shift nearly 400 as when the peak intensity changes from 1×10^{14} W/cm^2 to 5×10^{14} W/cm^2. For a better comparison, the differences of the BRTs between the Ar and Xe potentials $\Delta t_r^{\mathrm{XA}} = t_r^{\mathrm{Xe}} - t_r^{\mathrm{Ar}}$ are shown in Fig. 3(c). The differences Δt_r^{XA} were positive for the intensities from 1×10^{14} to 5×10^{14} W/cm^2 and are a decreasing function of the intensity. We can, therefore, make two conclusions from these observations. One is that the stronger the attractive force of the parent ion is, the earlier the BRT of the electron is. The other is that the BRTs are changed by the peak intensity dominantly over the ionization potential in the tunneling ionization regime.

C. Potential range and center wavelength dependence

After tunneling, the electron is driven by the laser field in the presence of the atomic field. Thus, the electron trajectory can be changed by the spatial profile of the atomic field. We compared the classical backpropagation results obtained with a soft-core potential and a soft-core Yukawa potential, which is defined as

$$V(x) = -\frac{e^{-b\sqrt{x^2+a}}}{\sqrt{x^2+a}}, \tag{2}$$

where $b \geqslant 0$ determines the range of the potential. The potential becomes increasingly short ranged as the parameter b increases. For a given b, the parameter a was adjusted to fix the ionization potential to that of Ar. As a result, the soft-core Yukawa potential with non-zero b is narrower and deeper than the soft-core potential ($b = 0$).

The BRTs were calculated for different b values and the peak intensities of the laser field, as shown in Fig. 4. The BRTs near the cutoff momentum for $b = 0$ (solid lines, identical to the soft-core potential) and $b = 2$ (dashed lines) are shown in Fig. 4(a). The BRTs for $b = 2$ are later than those for $b = 0$ for the peak intensities from 1.0×10^{14} to 5.0×10^{14} W/cm^2. The rescattering times obtained for $b = 2$ and $b = 0$ shift by a few hundred attoseconds as the peak intensity increases. Thus, it can be concluded that shifts of a few hundreds of attosecond in the BRTs shown in Figs. 3(b) and 4(a) are due to the peak intensity dependence of the rescattering dynamics before the rescattering time. The shape of the potential is an important factor at relatively low intensities, around 1.0×10^{14} W/cm^2, but it is less important when the peak intensity is high.

To compare the BRTs obtained for different b values and the peak intensities in detail, we chose a specific momentum, 0.4 atomic units relative to p_{cutoff} at each intensity, as shown in Figs. 4(a) (black dot-dashed line) and 4(b). The BRTs are earlier for the soft-core Coulomb potential ($b = 0$) than those for the soft-core Yukawa potential with non-zero b values for all the peak intensities, as shown in the inset in Fig. 4(b). We set the soft-core potential ($b = 0$) as a reference and show the difference $\Delta t_r^{\mathrm{YS}} = t_r^{\mathrm{Yukawa}} - t_r^{\mathrm{Soft}}$ in Fig. 4(c). For all the peak intensities and b values shown in Fig. 4(c), Δt_r^{YS} are positive. These observations show that the BRTs depend on the width of the core, and the electron rescatters earlier in a shallow and wide potential than a deep and narrow potential. Similar to the results shown in Fig. 3, Δt_r^{YS} is a decreasing function of the peak intensity [Fig. 4(c)]. It shows that the BRT is predominantly determined by the intensity of the laser pulse and it is less sensitive to the potential profile of the parent ion.

Since the travel distance of the electron between the ionization time and the rescattering time depends on the center

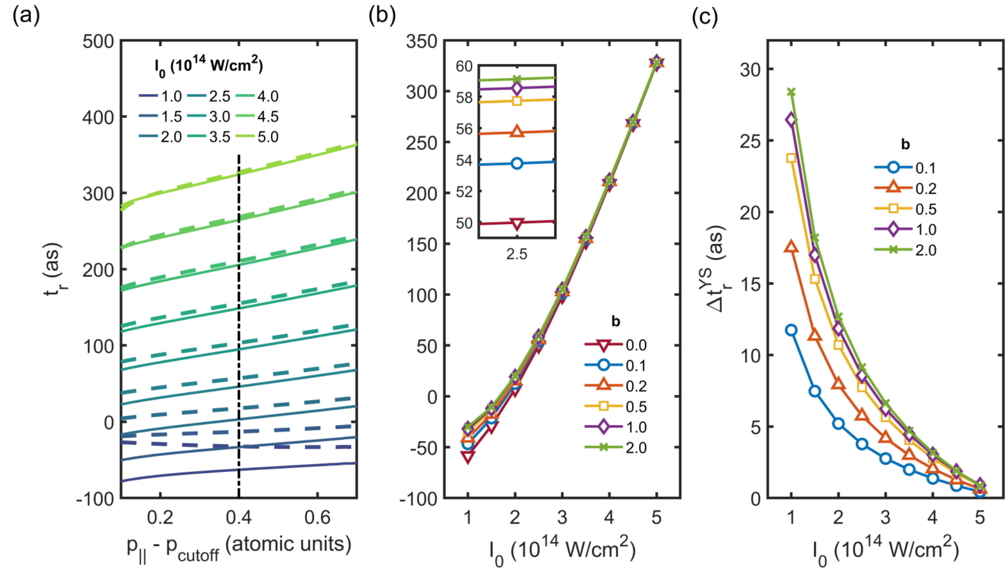

FIG. 4. Peak intensity dependence of BRTs in the soft-core Yukawa potential. (a) BRTs as a function of momentum near the cutoff momentum for each peak intensity. Solid lines are BRTs obtained for $b = 0$, and dashed lines corresponds to BRTs obtained for $b = 2$. (b) BRTs obtained for different b values at 0.4 atomc units in momentum relative to the classical cutoff momentum denoted by dotted-dashed line shown in (a). Inset: a magnified plot near $I_0 = 2.5 \times 10^{14}$ W/cm^2. (c) BRTs shown in (b) relative to the BRTs in soft-core potential without the exponential factor, which is equivalent to $b = 0$.

wavelength of the driving laser pulse, the BRT is also affected by the center wavelength. We calculated the BRTs for different center wavelengths in Ar, as shown in Fig. 5. We set the CEP of 0.5π and compared the BRTs near the zero-crossing time of the laser field ($t = 0$). The peak intensity of the laser fields was adjusted so that the ponderomotive energy of an electron is fixed to 12 eV and the Keldysh parameter $\gamma = \sqrt{I_p/2U_p}$ is not changed. The length of the rescattering trajectory predicted by the equation (1) is proportional to $E_0\lambda^2$ so that the length of the trajectory is proportional to the center wavelength for the fixed ponderomotive energy. The BRTs are earlier for the long center wavelengths in the SMM because in the case of the SMM the BRT is scaled as $t_r \propto \lambda$, (as follows from the equation (1)). The BRTs obtained by the classical backpropagation for the short center wavelengths are later than the zero-crossing time of the electric field. Since we fixed the ponderomotive energy, the intensity increases as the wavelength decreases. Therefore, this wavelength dependence of the BRT when the ponderomotive energy is fixed can be explained by the peak intensity dependence observed in Figs. 3 and 4.

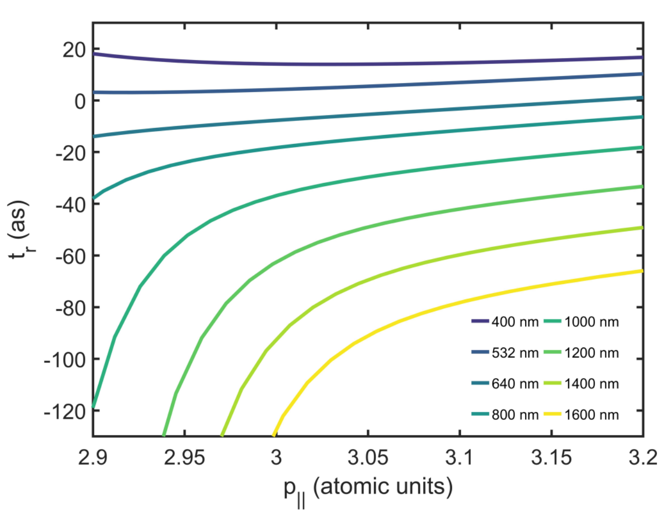

FIG. 5. Center wavelength dependence of BRTs in Ar soft-core potential. Ponderomotive energy of the electron is fixed to 12 eV so that peak intensity of the laser field is adjusted accordingly. The legend denotes center wavelength of the laser pulse used for each result.

We have analyzed dependence of the BRTs on various atomic and laser parameter as CEP, wavelength, ionic potential shape, and peak intensity using the classical backpropagation method. While the BRT is sensitive to all these parameters, the peak intensity of the driving laser pulse plays the crucial role. The difference of the BRTs for different shapes of the potential is an order of 10 as, as shown Figs. 3 and 4. If the long range part of the Coulomb potential is the main factor for the peak intensity dependence, the BRTs obtained in the Yukawa potential should be delayed by a few hundreds of attoseconds compared to that of the Coulomb potential. The peak intensity dependence of BRTs obtained for different soft-core Yukawa potentials with various ranges are similar to the soft-core potential. Since we consider the potential during the backpropagation, the peak intensity dependence of the BRTs should be related to the electron dynamics before rescattering time. Therefore, knowledge of the electron dynamics before rescattering is required to investigate the peak intensity dependence.

Unfortunately, we cannot access the electron dynamics before rescattering using the backpropagation method. To do that, we should be able to start the backpropagation from the classically forbidden momentum and position (i.e., beyond the cutoff). Also, it is difficult to describe reliably the rescattering dynamics classically. In order to find the electron trajectory before rescattering, one can assume that elastic backscattering occurs at $x = 0$. On the other hand, one can consider an orbiting trajectory for rescattering. These electron trajectories are totally different. Even if we set the rescattering conditions properly, the local classical electron trajectory cannot fully describe the rescattering process where which-way information (forward rescattering or backward rescattering) is lacked in the solution of the TDSE. Thus, although the backpropagation method that we presented yields reasonable estimations on the rescattering times, it cannot be used to access the electron dynamics before rescattering.

IV. DISCUSSION

In summary, we have shown that the backward rescattering time (BRT) of a tunnel-ionized electron in an intense laser field can be determined using the classical backpropagation method. The backpropagation method provides a consistent way to determine the rescattering time. We analyzed the dependence of the BRTs on various parameters such as the carrier envelope phase (CEP), ionization potential, peak intensity, potential shape, and center wavelength. The BRT is affected by all these parameters. The BRTs are distributed near the zero-crossing time of the electric field. They vary as the CEP of the driving laser pulse changes as expected on the basis of the treatment provided by the simple man model (SMM). The backward rescattering occurs earlier for systems with higher ionization potentials. The shape of the ionic potential also affects the BRT. The backward rescattering occurs earlier for a steeper potential of the parent ion.

We find that the peak intensity is the most important factor which determines the BRT. While the rescattering time is changed by a few or few tens of attoseconds for different ionization potentials, profiles and wavelengths, it is changed by a few hundred attoseconds when the peak intensity is varied from 1×10^{14} to 5×10^{14} W/cm^2. The rescattering time is a key parameter to describe the ultrafast electron dynamics in the intense laser field. We note that the backpropagation method can be applied using 2D models or 3D models. Consequently, the sensitivity of the rescattering times to the various parameters, and especially the peak intensity of the laser field should be carefully considered in applications in which knowledge of the rescattering time is important, such as laser-induced electron diffraction (LIED), high-order harmonic generation (HHG), and attosecond holography.

[1] R. R. Freeman, P. H. Bucksbaum, H. Milchberg, S. Darack, D. Schumacher, and M. E. Geusic, Above-Threshold Ionization with Subpicosecond Laser Pulses, Phys. Rev. Lett. **59**, 1092 (1987).

[2] P. B. Corkum, N. H. Burnett, and F. Brunel, Above-Threshold Ionization in the Long-Wavelength Limit, Phys. Rev. Lett. **62**, 1259 (1989).

[3] P. B. Corkum, Plasma Perspective on Strong Field Multiphoton Ionization, Phys. Rev. Lett. **71**, 1994 (1993).

[4] P. B. Corkum, C. Rolland, and T. Srinivasan-Rao, Supercontinuum Generation in Gases, Phys. Rev. Lett. **57**, 2268 (1986).

[5] O. Smirnova, Y. Mairesse, S. Patchkovskii, N. Dudovich, D. Villeneuve, P. Corkum, and M. Yu. Ivanov, High harmonic interferometry of multi-electron dynamics in molecules, Nature (London) **460**, 972 (2009).

[6] H. J. Wörner, J. B. Bertrand, D. V. Kartashov, P. B. Corkum, and D. M. Villeneuve, Following a chemical reaction using high-harmonic interferometry, Nature (London) **466**, 604 (2010).

[7] K. T. Kim, C. Zhang, A. D. Shiner, B. E. Schmidt, F. Légaré, D. M. Villeneuve, and P. B. Corkum, Petahertz optical oscilloscope, Nat. Photonics **7**, 958 (2013).

[8] K. T. Kim, C. Zhang, T. Ruchon, J.-F. Hergott, T. Auguste, D. M. Villeneuve, P. B. Corkum, and F. Quéré, Photonic streaking of attosecond pulse trains, Nat. Photonics **7**, 651 (2013).

[9] T. J. Hammond, G. G. Brown, K. T. Kim, D. M. Villeneuve, and P. B. Corkum, Attosecond pulses measured from the attosecond lighthouse, Nat. Photonics **10**, 171 (2016).

[10] T. Gaumnitz, A. Jain, Y. Pertot, M. Huppert, I. Jordan, F. Ardana-Lamas, and H. J. Wörner, Streaking of 43-Attosecond soft-X-Ray pulses generated by a passively CEP-stable mid-infrared driver, Opt. Express **25**, 27506 (2017).

[11] L. Quintard, V. Strelkov, J. Vabek, O. Hort, A. Dubrouil, D. Descamps, F. Burgy, C. Péjot, E. Mével, F. Catoire, and E. Constant, Optics-less focusing of XUV high-order harmonics, Sci. Adv. **5**, eaau7175 (2019).

[12] T. Nubbemeyer, K. Gorling, A. Saenz, U. Eichmann, and W. Sandner, Strong-Field Tunneling without Ionization, Phys. Rev. Lett. **101**, 233001 (2008).

[13] J. McKenna, S. Zeng, J. J. Hua, A. M. Sayler, M. Zohrabi, N. G. Johnson, B. Gaire, K. D. Carnes, B. D. Esry, and I. Ben-Itzhak, Frustrated tunneling ionization during laser-induced D 2 fragmentation: Detection of excited metastable D* Atoms, Phys. Rev. A **84**, 043425 (2011).

[14] H. Yun, J. H. Mun, S. I. Hwang, S. B. Park, I. A. Ivanov, C. H. Nam, and K. T. Kim, Coherent extreme-ultraviolet emission generated through frustrated tunnelling ionization, Nat. Photonics **12**, 620 (2018).

[15] G. G. Paulus, W. Nicklich, H. Xu, P. Lambropoulos, and H. Walther, Plateau in above Threshold Ionization Spectra, Phys. Rev. Lett. **72**, 2851 (1994).

[16] G. Paulus, F. Grasbon, H. Walther, P. Villoresi, M. Nisoli, S. Stagira, E. Priori, and S. De Silvestri, Absolute-phase phenomena in photoionization with few-cycle laser pulses, Nature (London) **414**, 182 (2001).

[17] F. Lindner, M. G. Schätzel, H. Walther, A. Baltuška, E. Goulielmakis, F. Krausz, D. B. Milošević, D. Bauer, W. Becker, and G. G. Paulus, Attosecond Double-Slit Experiment, Phys. Rev. Lett. **95**, 040401 (2005).

[18] D. B. Milošević, G. G. Paulus, D. Bauer, and W. Becker, Above-Threshold ionization by few-cycle pulses, J. Phys. B **39**, R203 (2006).

[19] T. Wittmann, B. Horvath, W. Helml, M. G. Schätzel, X. Gu, A. L. Cavalieri, G. G. Paulus, and R. Kienberger, Single-shot carrier–envelope phase measurement of few-cycle laser pulses, Nat. Phys. **5**, 357 (2009).

[20] M. Richter, M. Kunitski, M. Schöffler, T. Jahnke, L. P. H. Schmidt, M. Li, Y. Liu, and R. Dörner, Streaking Temporal Double-Slit Interference by an Orthogonal Two-Color Laser Field, Phys. Rev. Lett. **114**, 143001 (2015).

[21] T. Zuo, A. Bandrauk, and P. B. Corkum, Laser-induced electron diffraction: a new tool for probing ultrafast molecular dynamics, Chem. Phys. Lett. **259**, 313 (1996).

[22] M. Meckel, D. Comtois, D. Zeidler, A. Staudte, D. Pavicic, H. C. Bandulet, H. Pepin, J. C. Kieffer, R. Dorner, D. M. Villeneuve, and P. B. Corkum, Laser-induced electron tunneling and diffraction, Science **320**, 1478 (2008).

[23] M. Peters, T. T. Nguyen-Dang, C. Cornaggia, S. Saugout, E. Charron, A. Keller, and O. Atabek, Ultrafast molecular imaging by laser-induced electron diffraction, Phys. Rev. A **83**, 051403 (2011).

[24] M. Peters, T. T. Nguyen-Dang, E. Charron, A. Keller, and O. Atabek, Laser-induced electron diffraction: A tool for molecular orbital imaging, Phys. Rev. A **85**, 053417 (2012).

[25] M. G. Pullen, B. Wolter, A.-T. Le, M. Baudisch, M. Hemmer, A. Senftleben, C. D. Schröter, J. Ullrich, R. Moshammer, and C.-D. Lin, and others, Imaging an aligned polyatomic molecule with laser-induced electron diffraction, Nat. Commun. **6**, 7262 (2015).

[26] B. Bergues, M. Kübel, N. G. Johnson, B. Fischer, N. Camus, K. J. Betsch, O. Herrwerth, A. Senftleben, A. M. Sayler, T. Rathje, T. Pfeifer, I. Ben-Itzhak, R. R. Jones, G. G. Paulus, F. Krausz, R. Moshammer, J. Ullrich, and M. F. Kling, Attosecond tracing of correlated electron-emission in non-sequential double ionization, Nat. Commun. **3**, 813 (2012).

[27] A. Chen, M. Kübel, B. Bergues, M. F. Kling, and A. Emmanouilidou, Non-sequential double ionization with near-single cycle laser pulses, Sci. Rep. **7**, 7488 (2017).

[28] G. P. Katsoulis and A. Emmanouilidou, Fingerprints of slingshot non-sequential double ionization on two-electron probability distributions, Sci. Rep. **9**, 18855 (2019).

[29] K. Varjú, Y. Mairesse, P. Agostini, P. Breger, B. Carré, L. J. Frasinski, E. Gustafsson, P. Johnsson, J. Mauritsson, H. Merdji, P. Monchicourt, A. L'Huillier, and P. Salières, Reconstruction of Attosecond Pulse Trains Using an Adiabatic Phase Expansion, Phys. Rev. Lett. **95**, 243901 (2005).

[30] K. Zhao, Q. Zhang, M. Chini, Y. Wu, X. Wang, and Z. Chang, Tailoring a 67 attosecond pulse through advantageous phase-mismatch, Opt. Lett. **37**, 3891 (2012).

[31] U. S. Sainadh, H. Xu, X. Wang, A. Atia-Tul-Noor, W. C. Wallace, N. Douguet, A. Bray, I. Ivanov, K. Bartschat, A. Kheifets, R. T. Sang, and I. V. Litvinyuk, Attosecond angular streaking and tunnelling time in atomic hydrogen, Nature (London) **568**, 75 (2019).

[32] W.-C. Jiang, S.-G. Chen, L.-Y. Peng, and J. Burgdörfer, Two-Electron Interference in Strong-Field Ionization of He by a Short Intense Extreme Ultraviolet Laser Pulse, Phys. Rev. Lett. **124**, 043203 (2020).

[33] P. Botheron and B. Pons, Self-consistent bohmian description of strong field-driven electron dynamics, Phys. Rev. A **82**, 021404(R) (2010).

[34] R. Sawada, T. Sato, and K. L. Ishikawa, Analysis of strong-field enhanced ionization of molecules using bohmian trajectories, Phys. Rev. A **90**, 023404 (2014).

[35] N. Douguet and K. Bartschat, Dynamics of tunneling ionization using bohmian mechanics, Phys. Rev. A **97**, 013402 (2018).

[36] M. Li, J.-W. Geng, H. Liu, Y. Deng, C. Wu, L.-Y. Peng, Q. Gong, and Y. Liu, Classical-Quantum Correspondence for Above-Threshold Ionization, Phys. Rev. Lett. **112**, 113002 (2014).

[37] K. Amini, J. Biegert, F. Calegari, A. Chacón, M. F. Ciappina, A. Dauphin, D. K. Efimov, C. Figueira de Morisson Faria, K. Giergiel, P. Gniewek, A. S. Landsman, M. Lesiuk, M. Mandrysz, A. S. Maxwell, R. Moszyński, L. Ortmann, J. Antonio Pérez-Hernández, A. Picón, E. Pisanty, J. Prauzner-Bechcicki, K. Sacha, N. Suárez, A. Zaïr, J. Zakrzewski, and M. Lewenstein, Symphony on strong field approximation, Rep. Prog. Phys. **82**, 116001 (2019).

[38] A. S. Maxwell and C. F. de Morisson Faria, Coulomb-free and coulomb-distorted recolliding quantum orbits in photoelectron holography, J. Phys. B **51**, 124001 (2018).

[39] H. Ni, U. Saalmann, and J.-M. Rost, Tunneling Ionization Time Resolved by Backpropagation, Phys. Rev. Lett. **117**, 023002 (2016).

[40] H. Ni, U. Saalmann, and J.-M. Rost, Tunneling exit characteristics from classical backpropagation of an ionized electron wave packet, Phys. Rev. A **97**, 013426 (2018).

[41] H. Ni, N. Eicke, C. Ruiz, J. Cai, F. Oppermann, N. I. Shvetsov-Shilovski, and L.-W. Pi, Tunneling criteria and a nonadiabatic term for strong-field ionization, Phys. Rev. A **98**, 013411 (2018).

[42] K. Liu, H. Ni, K. Renziehausen, J.-M. Rost, and I. Barth, Deformation of Atomic p± Orbitals in Strong Elliptically Polarized Laser Fields: Ionization Time Drifts and Spatial Photoelectron Separation, Phys. Rev. Lett. **121**, 203201 (2018).

[43] H. Ni, S. Brennecke, X. Gao, P.-L. He, S. Donsa, I. Březinová, F. He, J. Wu, M. Lein, X.-M. Tong, and J. Burgdörfer, Theory of Subcycle Linear Momentum Transfer in Strong-Field Tunneling Ionization, Phys. Rev. Lett. **125**, 073202 (2020).

[44] G. G. Paulus, W. Becker, W. Nicklich, and H. Walther, Rescattering effects in above-threshold ionization: A classical model, J. Phys. B **27**, L703 (1994).

[45] Y. H. Kim, I. A. Ivanov, S. I. Hwang, K. Kim, C. H. Nam, and K. T. Kim, Attosecond streaking using a rescattered electron in an intense laser field, Sci. Rep. **10**, 22075 (2020).

[46] B. Feuerstein and U. Thumm, On the computation of momentum distributions within wavepacket propagation calculations, J. Phys. B **36**, 707 (2003).